Study of Polyanilines by High-Resolution Electron Microscopy

Léo Mazerolles,[†] Sandrine Folch,[‡,§] and Philippe Colomban*[,‡,§]

CECM, CNRS, 14 rue Georges Urbain, 94407 Vitry-sur-Seine, France; LADIR, CNRS-Université Pierre et Marie Curie, 2 rue Henry Dunant 94320 Thiais, France; and DMSC, ONERA, BP 72, 92322 Chatillon, France

Received August 3, 1999; Revised Manuscript Received October 1, 1999

ABSTRACT: A chemically prepared emeraldine chloride powder has been studied by high-resolution electron microscopy. Two kinds of grains with varying degrees of crystallinity were observed: (i) Rolled sheets (20−100 nm in diameter) (aggregates, disks, or ribbons ?) with an amorphous surface layer are identified as the EB-II polymer polymorph because of the centering of the cell and characteristic interreticular distances. A periodicity (∼5 nm) ascribed to the growth irregularity of the pristine polymeric aggregate is observed around the catalytic center. (ii) Crystalline grains (20−50 nm) exhibiting well-characterized 0.59-nm interreticular spacing are identified as the ES-I emeraldine salt. The interchain structural order appears stronger than the order along the polyaniline chain, according to the bond angle flexibility. The observed concentric nanostructure supports both the sketch of ordered islands and the paracrystal descriptions.

Introduction

The short-range order and disorder within conducting polymers and especially polyaniline (PANI) remains the subject of intense discussion. The conformation of the polymeric chain, the location of the anions, and the chain-to-chain and chain-to-anion packings are all aspects of the short-range order, which may determine the electric (electron and proton) conductivity. The effect of the disorder, and of the one dimensionality (1D) of the polymer, on the nature of the metallic state and on the insulator−metal transition are still strongly debated. To date, there is no precise knowledge of the structural and molecular arrangement. However, the crystallinity of PANI salts is 50% at best. The electrical and magnetic properties of PANI salts have been described schematically by metallic islands dispersed in a poorly conductive matrix[1] but no correspondence between metallic islands and crystalline regions have been be established to date. The Inhomogeneous Disorder Model treats the conducting polymers in the metallic state as composite systems of metallic, ordered, 3D regions, with delocalized charge carriers, and disordered, quasi-1D regions through which hopping transport occurs along and between the chains. The general formula describing the emeraldine polymer, the more stable form of the polyaniline chain, is $[(C_6H_4)NH(C_6H_4)-NH-]_{0.5}[(C_6H_4)N{=}(C_6H_4){=}N-]_{0.5}$. This polymeric semiconducting form, usually called emeraldine base EB-I is prepared by acid deintercalation of the conducting ES-I salt form synthesized by oxidative polymerization of aniline ($C_6H_5NH_2$) in 1 M aqueous HCl.[2,3] Another salt form (ES-II) is obtained from an emeraldine solution in anhydrous sulfuric or methane sulfuric acids[4] by precipitation with water, or methanol. Although the EB-I form obtained by leaching of an ES-I solution in 3 wt % ammoniac is amorphous, a more or less crystalline EB-II form can be prepared by dissolution−solvent evaporation in *N*-methylpyrrolidone (NMP) and then tetrahydrofurane (THF) or subsequent mechanical treatment (stretching,[5] grinding,[6] etc.). The corresponding ES-II salt is obtained after acid intercalation.

The first extensive X-ray structural studies of PANI short-range order have been reported by Pouget and coworkers.[5,7−10] Comparison of a few measured *d* spacing and Bragg intensities led to the identification of two polymorphic families, EB-I/ES-I and EB-II/ES-II. Vibrational spectroscopy also allows the distinction between the different classes of polyanilines, regardless of the anion.[11,12] The observation of bands at the same wavenumber on ES-II IR and Raman spectra reveals a noncentrosymmetric structure, as proposed by Pouget et al.[5] In contrast, the IR/Raman mutual exclusion for low wavenumber spectra of the ES-I form indicates its structure has a center of symmetry, in contradiction with Pouget's proposal. Besides, band-shape analysis ruled out the simple model of a pavement of amorphous and crystalline regions. A description using the "paracrystal model", i.e., a continuous deformation of the chain geometry, appears more adapted to describe the short-range disorder. However the chemical and structural flexibility of the nitrogen linkage between the aromatic cycles in the polymeric chain makes progressive deviation possible along the zigzag chain:[12] equal consecutive deviations lead to a linear chain segment with helical structure, while alternative equal deviations do not provide linear or compact chain segments, but an expanded coil (Figure 1).

The direct observation of the aromatic cycles, anions, and chain arrangement is mandatory for a real understanding of the local structure of the materials, in light of the partial conclusions given by the different methods of analysis. We report here a preliminary study on the emeraldine chlorine salt (ES-I) powder by high-resolution transmission electron microscopy.

Experimental Section

Samples Preparation. Pristine emeraldine hydrochloride powder (ES-I form) was synthesized at 3 °C by an oxidative polymerization of $C_6H_4{-}NH_2$ in 1 M aqueous HCl using

* Corresponding author. Fax: 33 1 49 78 13 23. E-mail: colomban@glvt-cnrs.fr.
† CECM, CNRS.
‡ LADIR, CNRS-Université Pierre et Marie Curie.
§ DMSC, ONERA.

10.1021/ma991290a CCC: $18.00
Published on Web 11/13/1999

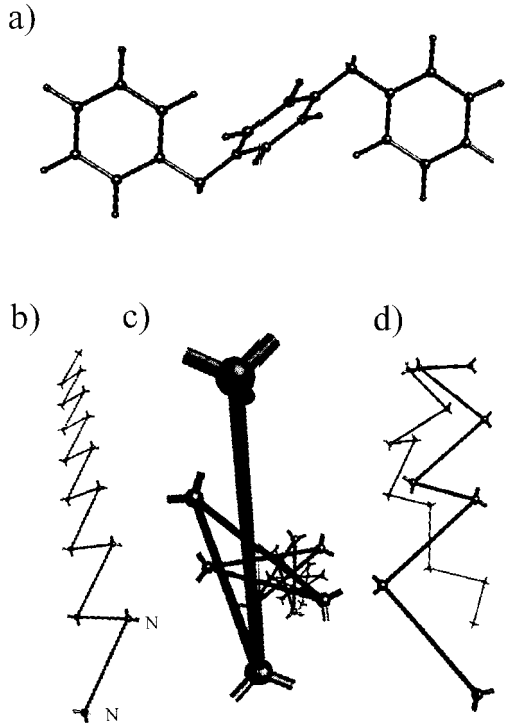

Figure 1. Sketch of the conformational variations of emeraldine chains allowed by orientational disorder and flexibility of the aromatic cycle−nitrogen bond. Part a shows the possible rotation of the N−aromatic cycle−N plane. The N−aromatic cycle−N segment is considered as a rigid virtual bond which forms linear zigzags (b), helical chains (c), or buckle chains (d).

ammonium peroxydisulfate as oxidant (aniline/oxidant molar ratio = 2), according to the method of Cao et al.[13] Details are given elsewhere.[12] The materials selected for TEM observation were chosen among those exhibiting well-defined low wavenumber Raman spectra.

Techniques. Crystalline phases were identified by X-ray diffraction (PHILIPS PW1710 diffractometer) using the filtered Kα radiation of a cobalt target.

The transmission electron microscopy (TEM) study was carried out on a TOPCON 002B microscope (C_s = 0.4 mm) fitted with a small-angle double-tilt stage (±10°) and operating at 200 kV. Specimens were prepared by softly crushing small quantities of the samples in ethanol (in an agate mortar) and then allowing a drop of the resulting suspension to dry on a perforated carbon film. Thin regions of flakes overhanging a hole in the carbon film were then chosen for observation. Numerical treatment by Fourier transform of some TEM images was performed after digitization of the experimental images with a charge-coupled device camera.

Results

TEM Observations. The study of the pristine emeraldine hydrochloride samples (mainly of the ES-I form according to Raman scattering and X-ray diffraction) by high-resolution transmission electron microscopy (HRTEM) reveals two kinds of regions, according to the level of organization:

(i) Well-organized regions exhibit curved fringes, as shown on Figure 2a,b. They look like sheets rolled around an axis (or circles around a center ?) and viewed in projection (section ?) along the electron beam axis. These fringes show the atomic planes of the structure. Their spacing does not vary and is close to 0.34 nm, which corresponds to the distance between the dense atomic planes (containing the aromatic cycles) for all the structures defined by Pouget and co-workers:[5,6] (110)

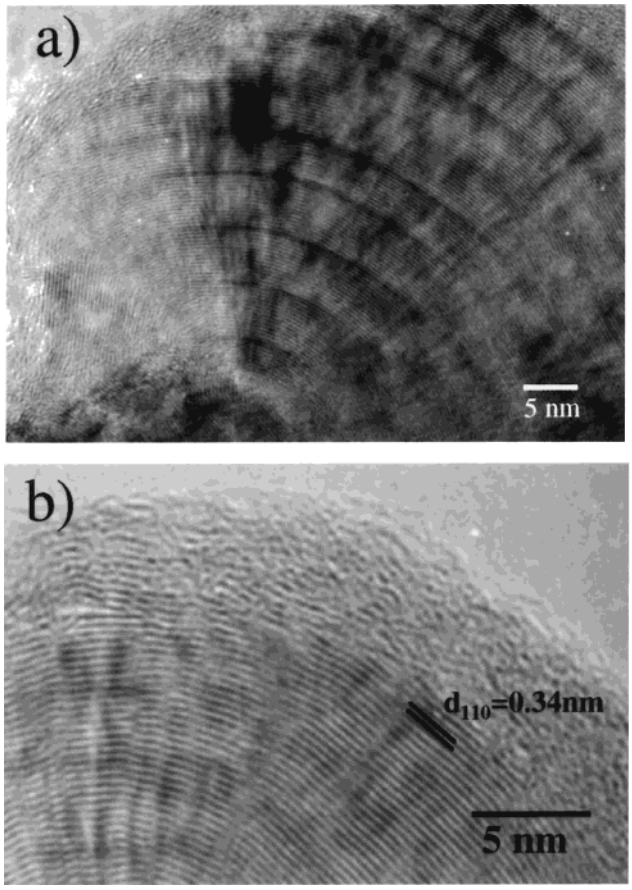

Figure 2. HRTEM images of a well-organized region in an ES-I sample exhibiting concentric regular planes (a) and the amorphous layer on the edge of the ordered zone (b).

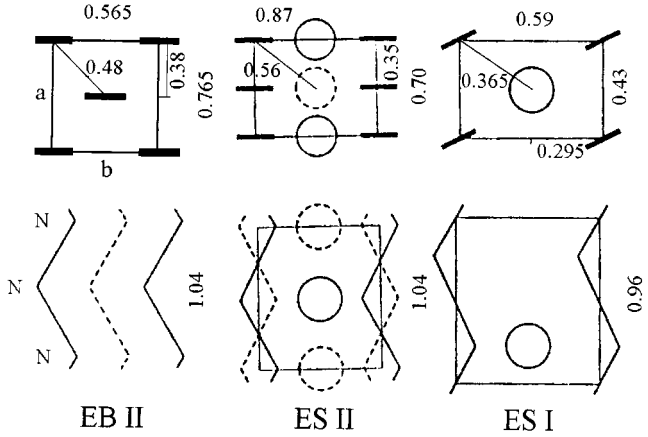

Figure 3. Scheme of the different unit cells on the (*a*,*b*) and (*c*,*b*) plane projections proposed by Pouget et al.[5] for EB-II, ES-II, and ES-I polymorphs. Large circles represent the anions.

planes for the ES-I structure and (200) planes for the EB-II and ES-II structures (schematic representations of the various unit cells proposed by Pouget et al.[5] are given in Figure 3). The atomic rows are concentric, with a diameter ranging from 20 to 100 nm. This diameter has to be related to the correlation distance measured for the narrower peaks (e.g., the 110 line corresponding to the chain-to-chain or chain-to-anion packing) from X-ray diffraction patterns using Scherer's formula.[6] It is not possible to say if the organized regions correspond to disks, ribbons, tubes, or simply aggregates. An amorphous layer of ∼5 nm thick is

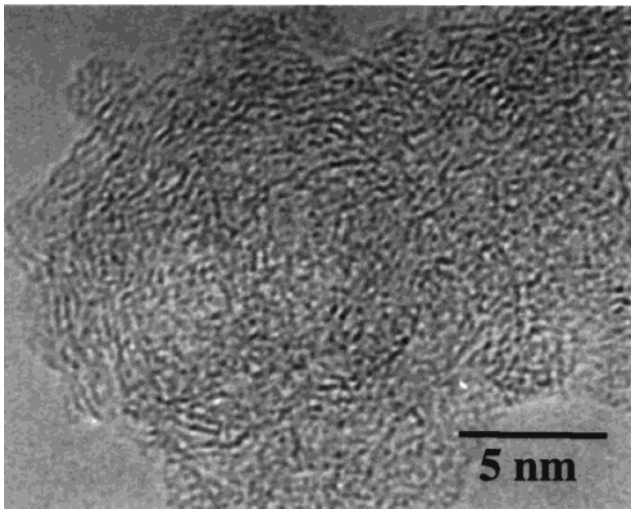

Figure 4. HRTEM image of an amorphous zone.

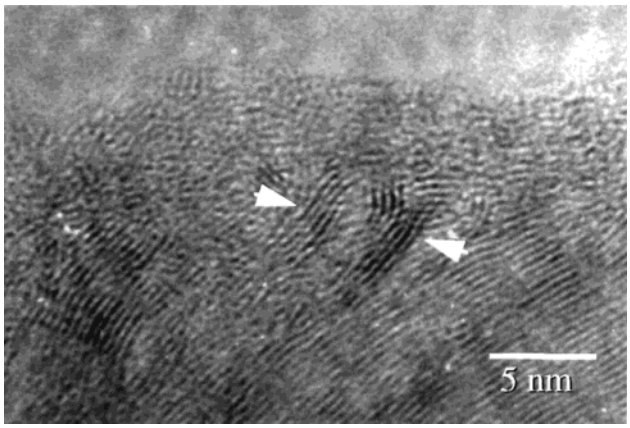

Figure 5. HRTEM image of the transition between disordered and well-organized zones. White arrows show distorted planes in the structure.

observed (Figure 2b), on the edge of these "nodules". Elsewhere, other regions, in the same specimen, display a contrast characteristic of less organized structures. In Figure 4 for instance, we observe a contrast typical of an amorphous structure. At the transition between the amorphous and periodic zones, series of three or four distorted atomic planes with a spacing of 0.34 nm are revealed (as shown by arrows in Figure 5). In the concentric regions, an additional darker contrast periodically appears along the fringes about every 5 nm (Figure 2a).

(ii) In other regions of the samples, grains with an irregular shape are also observed (Figure 6). Unfortunately, these grains are very unstable, under the electron beam, which reduces the quality of high-resolution images. It is likely that these grains correspond to the emeraldine salt and that their unstability under the electron beam is due to the loss of Cl^- anions as a result of heating during the observation. Their size is about 20−50 nm, and the measured interplanar distances are equal to $d = 0.59$ nm. We recall that this distance was observed on the X-ray diffraction patterns only in the case of ES-I forms, that is to say when an anion (Cl^-) is inserted in the structure of emeraldine. The X-ray powder patterns obtained on our materials are given in Figure 7. Peaks intensities and positions vary slightly, especially with water content.[6]

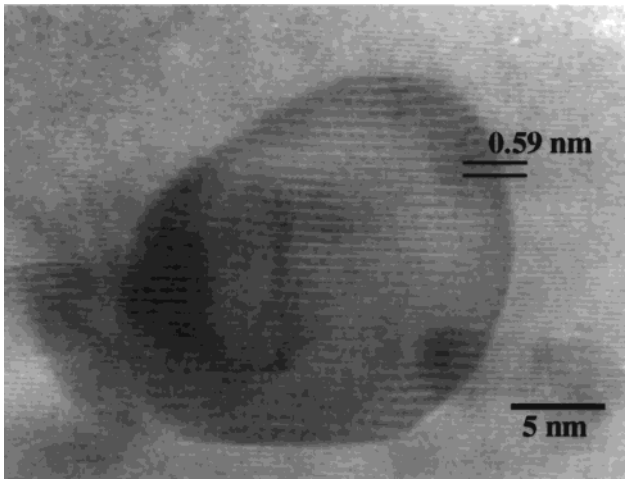

Figure 6. HRTEM image of aggregates.

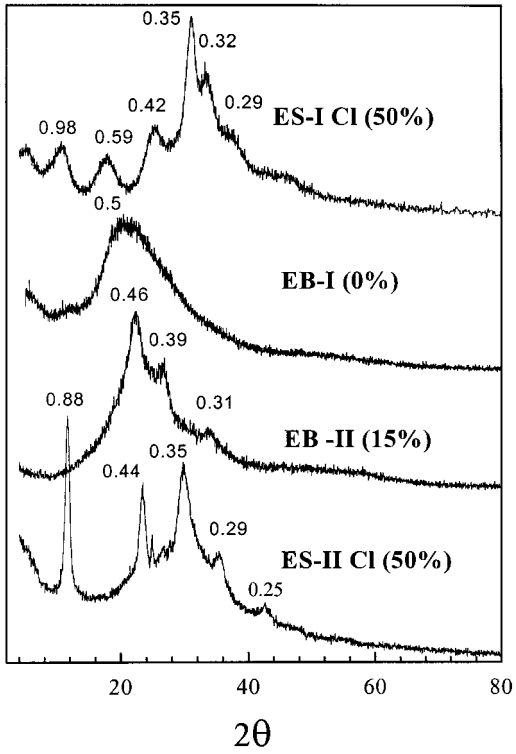

Figure 7. X-ray powder patterns of (a) ES-I pristine emeraldine salt, (b) EB-I emeraldine base, (c) EB-II emeraldine base, and (d) ES-II emeraldine salt. Crystallinity ratios are calculated after the fitting of the different peaks (see ref 12).

Discussion

The X-ray diffraction results show that the unit cell parameters vary slightly with authors and from batch-to-batch. For instance the data of Pouget et al.[5] are $a = 0.765$ nm, $b = 0.565$ nm, and $c = 1.04$ nm (EB-II form) and 0.43, 0.59, and 0.96 nm (ES-I form) while we obtained respectively 0.78, 0.57, and 1.07 nm (EB-II) and 0.42, 0.59, and 0.98 nm (ES-I). These differences could be attributed to the different water content and/or to some structural differences (e.g., the sequence of the aromatic cycle−nitrogen atom angles). Differences in peak-fitting procedure could also be invoked.

To interpret the HRTEM images it is important to remember that the pristine emeraldine salt is prepared in the form of an emeraldine hydrochloride powder with a composition close to $C_{24}H_{18}N_4 \cdot 2HCl \cdot 6H_2O$, after dry-

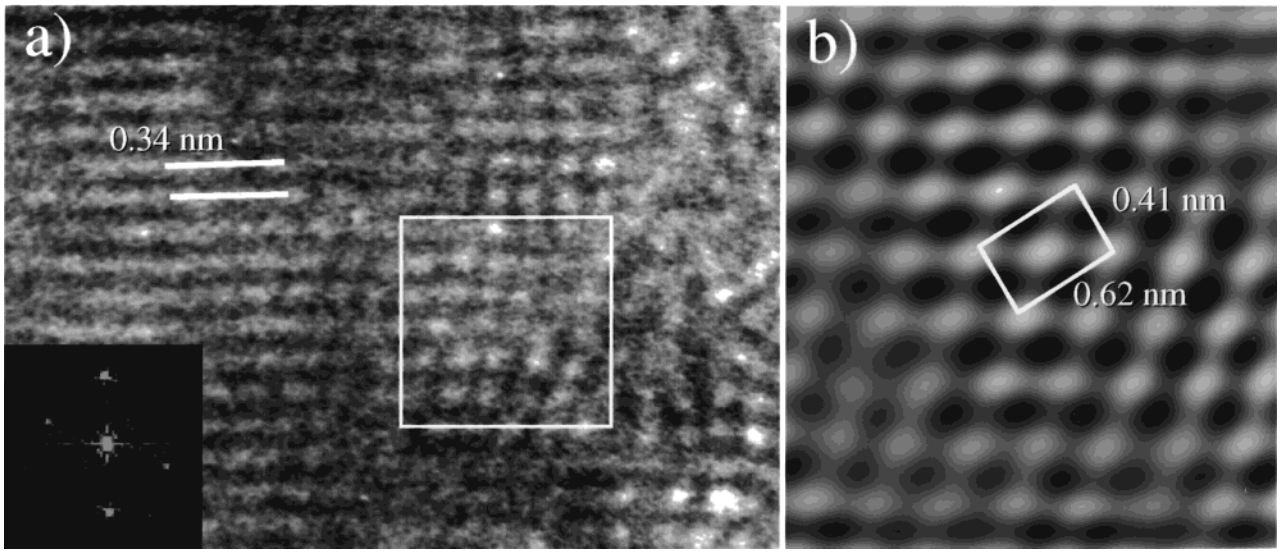

Figure 8. (a) HRTEM image of a region extracted from the concentric zones observed in Figure 2. The inset shows the numerical diffraction obtained from the modulus of the Fourier transform, revealing the periodicity in the selected area (indicated by a square) and (b) an image corresponding to the selected area in part a and reconstructed by inverse Fourier transform from the Bragg spots of the diffraction (Bragg filtering).

ing and equilibration in air at usual water partial pressure. Vacuum lowers the water content of the salt form to $4H_2O$ (drying under 10^{-2} Torr primary vacuum) or even less (long duration dynamic primary vacuum) and the thermal stability is weak, as observed for most hydrated proton conductors.[13] The combined deprotonation−dechlorination−dehydration process starts at about 50 °C[12,14] and is complete at 120 °C. For the high-vacuum conditions in the microscope, we expect the analyzed salts to lose all water molecules and a large amount of inserted chlorine anions. The observation of an amorphous contour would result from this quick loss of HCl and H_2O. The EB-I base is amorphous and retains only small amounts of water: $C_{24}H_{18}N_4 \cdot 0-0.5H_2O$. Solvent (THF) extraction of the short-chain fraction[5] and specific synthesis[12] can lead to the more crystallized EB-II base form. Its ability to retain water is not known, but we could expect that it is similar to that of the EB-I phase.

The periodic and concentric zones could correspond either to the ES forms or, after the loss of Cl^- anions positioned in the 110 planes (planes of nitrogen), to the EB-II form. In the inset of part a of Figure 8 is shown the numerical diffraction (modulus of the Fourier transform of the image) obtained from a part of the digitized high-resolution image. This powder spectrum was indexed using the cell parameters defined above and would correspond to the (001) plane. From this diffraction we reconstructed the image by inverse Fourier transform after selecting Bragg positions. This technique is used to enhance the contrast by elimination of the low frequencies (noise). The inset of part b shows the reconstructed image, and the drawn cell corresponds well to the one proposed by Pouget et al. for ES-II and EB-II (see Figure 3),[5] although its centering suggests a rearrangement occurs after the loss of Cl^- anions, giving EB-II form with a chain parallel to *c* axis at $^1/_2a$,$^1/_2b$. Pouget's model contains two variable parameters: the ring tilt angle ϕ and the polymer chain setting angle ψ. The variation of ψ (up to 30°) can explain the rotation of (110) planes inside the nodules described above. The interplane distances measured by electron microscopy are slightly shorter than those obtained by X-ray diffraction. This could originate from the shrinkage related to a more complete dehydration.

We cannot make a conclusion about the shape of the particle since it was not possible to obtain high-resolution images along a direction perpendicular to the plane of Figure 2. Due to atomic rows curvature, the part of the ordered region would have been very small (a few nanometers squared). Furthermore, its selection/occurrence would be difficult and rare. Not only the curvature and the small value of the correlation length along the 001 direction (chain axis) reduced the surface contributing to an image but faster amorphization was observed under the electron beam. In the later case, the heat and charge transfer must take place preferentially along the polymeric chain. When grains are oriented with chains parallel to the surface, the channeling of electrons by the structure and, consequently, the dissipation of the charge at the surface of the specimen must occur less rapidly than when the incident beam is parallel to the intrachain electron delocalization. Attempts to determine the length of the polymeric chain by chromatography concluded that standard length is equal to 100 nm and more ($M_n \sim 20\,000$ g mol^{-1} [3]) for EB-I and close to 10 nm ($M_n \sim 2000$ g mol^{-1}) for EB-II materials.[15] Thus, if the disk shape agrees well with the shorter chain length and with the assignment to EB-II form, a ribbon shape would be more consistent with the standard mean value. The tube shape can be rejected because we did not observe voids in the particle centers. At last, irregular nodule shape could tolerate various chain lengths.

The polymerization is catalyzed by the addition of ammonium peroxydisulfate and the aniline-to-oxidant ratio is a very important parameter for the achievement of a long-chained polymer.[3] Thus, we can expect polyaniline grains to grow around an active center due to the catalytic growth of polymeric chains. The regular grain size (20−80 nm) could correspond to the extent of the catalytic action. Typical molar masses are close to 20 000 g mol^{-1} with extremal values of 5000 and 40 0000 g mol^{-1},[16−18] which correspond to polymer lengths between 30 and 2000 nm. If we assume that the grain size is about the same order of magnitude than

the observed section, we effectively obtain chain lengths close to 300 nm. The darker contrast observed approximately every 5 nm on Figure 2 could originate from structural (projection of helical periodicity) or from chemical reasons. Cyclic reaction conditions are usually observed at the solid/liquid growth interface.[19]

Conclusion

HRTEM analysis confirms the considerable static disorder expected from X-ray diffraction and vibrational spectroscopy in polyanilines. The first stringent phenomenon is that the images are consistent with both the Inhomogeneous Disorder Model[1] and the paracrystal description,[12] proposed in the 1950s by Von Hoseman for other polymers.[20,21] The second important conclusion is that the interchain short-range order appears higher than the intrachain one. Attempts to show the materials parallel to the chain axis were unsuccessful. This is consistent with the very small correlation length (∼2 nm) calculated along this direction from the 001 Bragg peak.[6] The curved and concentric habit of Figure 2 looks similar to what was observed in layered silicates[22−26] with rolled or tubular structures and in carbon or boron nitride particles with onion or cone habit.[27]

The similarity of polyaniline X-ray powder patterns with those of fibrous materials such as halloysite, allophane, and chrysotile, for example, is obvious. All patterns show "tailed" reflections spread out in directions corresponding to increasing values of 2θ, which arise from the numerous stacking faults and from the curvature. The origin of rolled and tubular structures in silicates was first attributed by Pauling to the inherent misfits between the octahedra and tetrahedra sheets which contain various cations (e.g., Al/Mg) in octahedral and tetrahedral sites.[22] A similar mechanism can be expected in polyaniline with the alternation of nitrogen connected benzenic (C_6H_4-NH-) and quinoid ($C_6H_4-N=$) cycles causing internal stresses within and between the chains, due to the difference in bond length and charge. It has been emphasized that the sharp reflections from the above silicate systems require successive layers of the tubular systems to be ordered with respect to the tube axis. Any disorder in the way the layers are successively arranged would immediately reduce the sharpness of the reflections and peaks would be tailed. This would also explain the more or less regularly faulted black circles of Figure 2.

Acknowledgment. Drs A. Gruger, A. Regis, and D. Michel are kindly acknowledged for fruitful discussions.

References and Notes

(1) Kohlman, R. S.; Epstein, A. J. In Insulator−metal transition and inhomogeneous metallic state in conducting polymers. *Handbook of Conducting Polymers*; Marcel Dekker: New York, 1997; Chapter 3, pp 85−121.
(2) Jozefowicz, M.; Yu, L. T.; Perichon, J.; Buvet, R. *J. Polym. Sci.* **1969**, *C22*, 1187−1195.
(3) Cao, Y.; Andreatta, A.; Heeger, A. J.; Smith, P. *Polymer* **1989**, *30*, 2305−2311.
(4) Folch, S.; Gruger, A.; Régis, A.; Colomban, Ph. *Synth. Met.* **1996**, *81*, 221−225.
(5) Pouget, J. P.; Jozefowicz, M. E.; Epstein, A. J.; Tang, X.; MacDiarmid, A. G. *Macromolecules* **1991**, *24*, 779−789.
(6) Colomban, Ph.; Folch, S.; Gruger, A.; Régis, A.; Michel, D. *C. R. Acad. Sci. Paris IIb* **1996**, *322*, 63−70.
(7) Laridjani, M.; Pouget, J. P.; Scherr, E. M.; MacDiarmid, A. G.; Jozefowicz, M. E.; Epstein, A. J. *Macromolecules* **1992**, *25*, 4106−4113.
(8) Jozefowicz, M. E.; Leversanne, R.; Javerdi, H. H. S.; Epstein, A. J.; Pouget, J. P.; Tang, X.; MacDiarmid, A. G. *Phys. Rev. B* **1989**, *39*, 12958−12961.
(9) Pouget, J. P.; Jozefowicz, M. E.; Epstein, A. J.; Masters, J. G.; Ray, A.; MacDiarmid, A. G. *Macromolecules* **1991**, *24*, 5863−5866.
(10) Colomban, Ph.; Gruger, A.; Régis, A.; Michel, D. *J. Chim. Phys. (Paris)* **1995**, *92*, 951−954.
(11) Folch, S.; Gruger, A.; Colomban, Ph. *J. Chim. Phys. (Paris)* **1998**, *95*, 1299−1302.
(12) Colomban, Ph.; Folch, S.; Gruger, A. *Macromolecules* **1999**, *32*, 3080−3092.
(13) Colomban, Ph. Proton Conductors: Solids, membranes and gel. Materials and Devices; Cambridge Univerity Press: Cambridge, 1992.
(14) Hinrichs, R.; Gruger, A.; Régis, A.; Colomban, Ph. *Synth. Met.* **1996**, *81*, 227−239.
(15) Folch, S.; Régis, A.; Gruger, A.; Colomban, Ph. To be published.
(16) Moon, D. K.; Osakada, K.; Maruyama, T.; Yamamoto, T. *Makromol. Chem.* **1992**, *193*, 1723−1728.
(17) Davied, S.; Nicolau, Y. F.; Melis, F.; Revillon, A. *Synth. Met.* **1995**, *69*, 125−126.
(18) MacDiarmid, A. G.; Manohar, S. K.; Mattoso, L. H. C. U.S. Patent 789095-07, Nov 1991.
(19) Cox, G. A.; Ford, B. A. *J. Mater. Sci.* **1993**, *28*, 5637−5647.
(20) Hosemann, R. *Acta Crystallogr.* **1951**, *4*, 520−529.
(21) Guinier, A. In *Théorie et Technique de la Radiocristallographie*; Dunod: Paris 1956; p 617.
(22) Brindley, G. W., Brown, G., Eds. *Crystal structures of clay minerals and their X-ray identification*; Mineralogical Society Monograph no. 5, Mineralogical Society: London, 1980.
(23) Vali, H.; Köster, H. M. *Clay Miner.* **1986**, *21*, 827−859.
(24) Yada, K. *Acta Crystallogr.* **1967**, *23*, 704−707.
(25) Yada, K. *Acta Crystallogr.* **1971**, *A27*, 659−667.
(26) Henni, T.; Wada, K. *Am. Mineral.* **1976**, *61*, 379−390.
(27) Bourgeois, L.; Brando, Y.; Shinozaki, S.; Kurashima, K.; Sato, T. *Acta Crystallogr.* **1999**, *A55*, 168−177.

MA991290A